



Effective thermal conductivity of 3D-printed continuous wire polymer composites

Yehia Ibrahim¹ · Roger Kempers¹

Received: 11 August 2021 / Accepted: 26 December 2021 / Published online: 29 January 2022
© The Author(s), under exclusive licence to Springer Nature Switzerland AG 2022

Abstract

3D printing can be used to improve the geometric design of heat transfer structures by allowing the fabrication of more complex shapes which can enhance convective heat transfer; however, this can come at the expense of having a lower solid-phase thermal conductivity, especially when polymers are used. Improving the thermal conductivity of 3D-printed components has been the focus of many studies because of the potential to leverage additive manufacturing (AM) for thermal applications, such as heat exchangers. This study describes a fabrication process whereby 3D-printed polymer composites consisting of continuous metal wires and with enhanced effective thermal conductivity are fabricated using a modified fused filament fabrication (FFF) 3D printer. The wires were coextruded with the molten polymer through a modified hot end and nozzle assembly. The printed components have higher thermal conductivity than the base polymer because the wires create high thermal conductivity pathways in the printed rasters. Samples with different wire volume fractions, printing directions, and matrix materials were printed to investigate the effect of these parameters on the thermal conductivity of the printed composites. The thermal conductivity of the printed samples was evaluated experimentally using a steady-state measuring setup and analytically modeled using network thermal resistance models. The results show that 3D-printed continuous wire polymer composites can have a thermal conductivity as high as 9.4 W/mK using a volume fraction of 2.7% of continuous copper wires compared with 0.22 W/mK for the base polymer. Model results further demonstrate that usage of a higher volume fraction of conductive wires or other continuous conductive filler can further improve the thermal conductivity of these 3D-printed composites.

Keywords 3D-printed composite · Fused filament fabrication · Continuous fiber printing · Continuous wire polymer composites (CWPC) · Thermal conductivity

1 Introduction

Additive manufacturing (AM) offers significant freedom of design and the ability to create complex, high area-to-volume structures and lightweight heat exchange surfaces and structures. These manufacturing processes represent an opportunity to realize a new generation of polymer composite heat exchange and transfer technologies [1, 2]. Fabrication of polymer composites using AM techniques, such as 3D printing, has recently gained interest due to the advantages that 3D printing introduces to the manufacturing process [3, 4]. These include ease of manufacturing, high

precision, and the ability to fabricate complex geometries. Adding particle or fiber reinforcements into the polymer matrix permits fabrication of polymer-based composites, which are characterized by their higher mechanical and thermal performances [3, 4].

Fused filament fabrication (FFF) is one of most widely used techniques to 3D-print polymeric material; it is further used to fabricate polymer composites by mixing the polymeric material with reinforcement prior to the filament fabrication process. Metal fillers, such as iron and copper particles have been used as reinforcements for polymer matrixes, such as acrylonitrile butadiene styrene (ABS) and nylon. Generally, the addition of a higher volume fraction of metal filler particles results in lower tensile modulus, tensile stress, and elongation [5]; however, it improves thermal properties, such as the heat capacity and thermal conductivity of composites. Nikzad et al. [6] found that adding 10% volume

✉ Roger Kempers
kempers@yorku.ca

¹ Department of Mechanical Engineering, York University,
4700 Keele Street, Toronto M3J 1P3, Canada

fraction of iron particles increased the storage modulus by nearly 40% and that the glass transition temperature of the composite was seven degrees higher. They also found that the iron-ABS composite had significantly lower ultimate tensile strength (less than 50% of pure ABS). Masood et al. [7] found that increasing the volume fraction of iron particles in a nylon matrix further decreases the tensile strength of the composite. In addition, with the same filler volume fraction, the use of smaller metal particles results in lower ultimate tensile strength. In [8], they studied the effect of metal particle sizes on thermal conductivity and found that adding 40% volume fraction of fine iron particles resulted in a composite with five times higher thermal conductivity. Hwang et al. [9] also filled an ABS matrix with iron and copper particles with different volume fractions; they too found that the addition of both iron and copper particles results in a composite with lower tensile strength and higher thermal conductivity.

Fiber fillers are more commonly used with polymer composites because they offer significantly better mechanical properties. The filler, in the form of chopped fibers, can be easily mixed with the polymer to produce a printing filament [10]. Different types of fibers—such as carbon, Kevlar, and glass—were implemented to improve both thermal and mechanical properties. Zhong et al. [11] used glass fibers with different volume fractions as the reinforcement material in an ABS matrix. Ning et al. [12] investigated the effect of fused deposition modeling process parameters on the mechanical properties of carbon-fiber-reinforced ABS composites. Similarly, Ivey et al. [13] investigated the effect of a post-printing annealing procedure on the mechanical properties of both pure polylactic acid (PLA) and carbon-fiber-reinforced PLA composite. From a thermal standpoint, filler material, shape, and surface treatment can enormously affect the final thermal conductivity of composites [14]. Fillers with a high aspect ratio help to create bridges between the filler particles, facilitating phonon and electron transport within the composite, and subsequently increase the thermal conductivity [15]. Different types of fillers can also be mixed to bring the desired properties of each filler together [16].

The main challenge to improving thermal conductivity using discontinuous filler arises from the existence of interfacial thermal resistance between the filler and the matrix. Thermal contact resistance is caused by phonon scattering, and it must be minimized to increase thermal conductivity [17, 18]. It can be analytically described using theoretical models, such as the acoustic mismatch model [19]. Few experimental methods can be used to determine its value for different materials [20].

Substituting discontinuous fillers with a continuous phase can resolve discontinuous filler shortcomings. By the addition of continuous filler, a continuous network of conductive material in which heat is easily conducted is created. Ibrahim et al. showed that using continuous carbon fiber

with a nylon matrix can improve thermal conductivity of the polymer by up to 1000% at a fiber volume fraction of 34% [21]. This improvement in composite thermal conductivity can facilitate printing of more effective, corrosion-resistant, and lightweight heat exchangers [2, 22].

In a previous study, a 3D-printing technique was developed in which a continuous network of metal wires was introduced to a polymer matrix to fabricate continuous wire polymer composites (CWPCs) [23]. This technique was used to fabricate mechanically reinforced composites [24], strain sensors [25], and 3D-printed heaters [26]. The wire network can also be used to improve thermal conductivity of the composite by using highly conductive wires, such as copper, in the printing process. Therefore, the objective of the present study is to investigate the effective thermal conductivity of 3D-printed CWPCs with different configurations, matrix materials, and wire volume fractions.

2 CWPC parameters and fabrication

In the present study, the 3D-printed CWPCs were fabricated by coextruding continuous wires with the polymer matrix, using a modified 3D printer hot end, as shown in Fig. 1. The polymer filament was introduced to the heater block at an angle, and the wire was introduced to the molten polymer through a dispensing needle inserted into the heater block. The polymer and the wires were coextruded through the nozzle onto the moving build plate. Traction force pulled the wire out of the needle, creating rasters with embedded wires. This technique allows for different wire volume content and materials to be used.

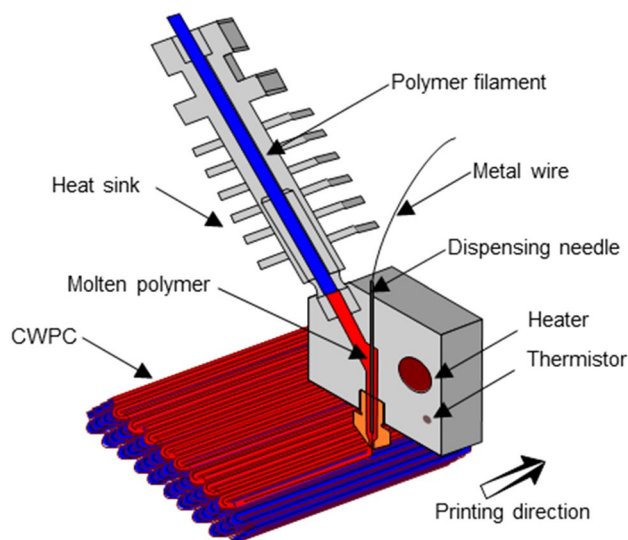


Fig. 1 Cross-sectional view of the modified 3D printer hot end head showing wire–polymer coextrusion technique

Additional details on the printing process can be found in [23, 24].

2.1 Wire properties

Different metal wires can be used with this manufacturing technique; however, copper and silver present the highest thermal conductivity of all metals, making them the best candidates to improve the thermal conductivity of the 3D-printed CWPCs. Copper wires are more commonly used for electrical applications and readily available in different sizes; thus, they were selected as continuous filler material in the present study.

The thermal conductivity of the 3D-printed CWPC depends on both the volume fraction and the geometry or orientation of the continuous wires. The volume fraction is dictated by both the wire diameter and nozzle diameter. A larger wire diameter at for a constant nozzle diameter increases the wire volume content and, subsequently, the thermal conductivity of the composite. However, it has been shown that the wire diameter should not exceed approximately 10% of the nozzle diameter to ensure sufficient polymer supports the wire, as described in [23]. In the present study, a 0.0762 mm (0.003 in) diameter copper (C110) wire was used (McMaster-Carr, Ohio, USA). Using this wire in conjunction with 0.6 mm and 1 mm diameter nozzles, two different wire volume fractions were studied.

These wires were uncoated to allow for potential thermal interaction between the wires and any discontinuous filler in the matrix materials which would further increase the thermal conductivity of the composite.

2.2 Printing parameters

The geometry and orientation of the continuous wires are dictated by the printing pattern of the CWPCs. Usually, preferable thermal performance is obtained in the direction parallel with the wire direction because the wires offer continuous paths for heat flow and less phase transitions between polymer and wire, thereby reducing interfacial resistances in the heat flow direction. Both factors increase the effective thermal conductivity.

To investigate directionality effects on the thermal conductivity of the CWPCs, two printing patterns were investigated: the first configuration is the unidirectional pattern in which the rasters in every layer are aligned in parallel, as shown in Fig. 2a. This pattern offers maximum thermal conductivity when the heat is conducted through the axis of the wires (parallel direction). However, in the transverse direction, minimal thermal conductivity will be obtained because the wire and polymer are in series [21]. The second configuration is the grid or bidirectional pattern, in which each layer of rasters is alternately printed such that every second layer of rasters is printed in the direction of heat flow and the others are printed in the transverse direction, as shown in Fig. 2b. Although this pattern sacrifices half of the conductive filler in the axial direction, it improves thermal conductivity in the transverse direction. This facilitates the fabrication of a material with similar in-plane thermal conductivities ($k_{xx} = k_{yy}$) which may be required in some thermal applications.

Other printing parameters, such as printing temperature and speed, have less effect on the thermal conductivity of the composite. These parameters tend to affect the mechanical properties of the composite more significantly by influencing

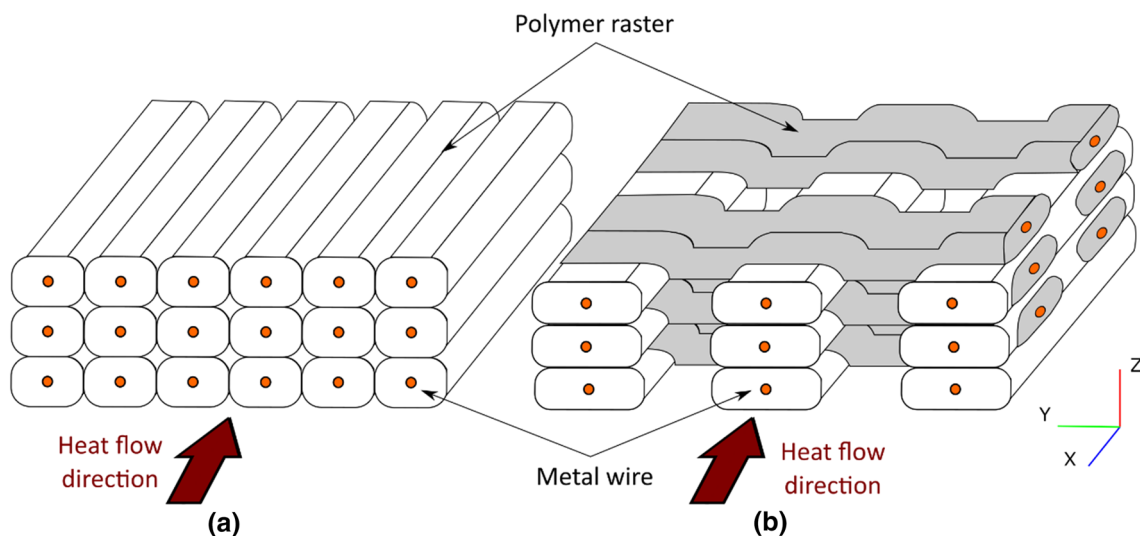


Fig. 2 Schematic of printing patterns: (a) unidirectional and (b) bidirectional

adhesion between rasters and air voids [13]. For CWPCs, interlayer matrix adhesion and air voids have minimal effect on thermal conductivity, especially when heat is conducted along the wires. The key printing parameters are summarized in Table 1.

2.3 Matrix materials

Matrix material also has a significant role on the thermal conductivity of the printed CWPC. In addition, the more conductive the matrix is, the less anisotropic the composite will be. Because the wire volume fraction is limited, increasing matrix thermal conductivity can further improve the thermal conductivity of the composite. Filament feedstock materials with discontinuous conductive fillers are commonly used to fabricate more durable and better-looking 3D-printed parts. These discontinuous fillers can also increase the thermal conductivity of the matrix, especially above the percolation ratio.

To investigate the effect of matrix material, a pure polymer and discontinuous polymer composite were used to characterize the influence of discontinuous filler on the thermal conductivity of the CWPC. Transparent PLA was chosen as the base matrix of the printed composites for its relative ease-of-printing and because its thermal conductivity has been well characterized [27]. The other matrix material was a discontinuous PLA composite, consisting of 80% copper particles. Although this percentage is not greater than the percolation threshold, it was anticipated that this matrix would present higher thermal conductivity than pure PLA. As such, we used a copper-filled PLA matrix to investigate the effect of the matrix on CWPC properties and explore any interaction between the continuous and discontinuous filler to further improve the composite thermal conductivity.

Table 1 Printing parameters

Parameter (units)	Nozzle diameter (mm)	
	0.6 mm	1.0 mm
Layer height (mm)	0.2	0.6
Raster width (mm)	0.65	1.05
Printing speed (mm/s)	10	10
Printing temperature (°C)	190	190
Printing angle (°)	0 or 0 & 90	0 or 0 & 90

Table 2 Matrix materials and suppliers

Matrix material + discontinuous filler	Supplier	Discontinuous filler content (volume %)	Filament diameter (mm)	Density (g/cm ³)
PLA	Spool 3D, Canada	–	1.75	1.25
PLA + copper	FormFutura, Netherlands	80	1.75	3.5

Additional details on these two matrix materials are presented in Table 2.

2.4 Sample dimensions

The outer dimensions of the printed samples were designed to fit the thermal conductivity measurement apparatus described below and had a cross-sectional dimension of 40 × 40 mm. The sample thickness was 25 mm in the direction of heat flow; this was then reduced in thickness by multiple stages of grinding and polishing to prepare the samples for testing. The geometries were designed using CAD software (SolidWorks 2017, Dassault Systems, Waltham, MA) and imported into printer slicing software (Slic3er, Prusa Research, Prague, Czech Republic) where printing parameters were selected and printing g-code was generated.

2.5 Sample configurations

Samples with different wire configurations, wire volume fractions, and matrix materials were printed to investigate the effect of these parameters on the thermal conductivity of the 3D-printed CWPCs; these are summarized in Table 3. One goal of this work is to increase the conductivity in the direction of the wires, with future 3D-printing methods potentially allowing for directionally controllable thermal conductivity. For this reason, most of the samples had the samples oriented unidirectionally. The bidirectional sample (Sample 4) used a standard grid pattern generated by the slicer whereby the raster direction is rotated by 90° within each layer as shown in Fig. 2b. Three replicate CWPC samples were printed to quantify test repeatability and the consistency of the printing process. Pure PLA and discontinuous copper-filled PLA matrix materials (Table 2) were printed to obtain the thermal conductivity of these base matrixes. The two matrixes were relatively homogenous and had isotropic properties, which meant that their thermal conductivities would not be affected by the printing pattern relative to the CWPCs.

2.6 Sample preparation and microscopy

The samples required smooth surfaces to minimize the effect of contact resistance between the samples and the test apparatus on the measured thermal conductivity. This

Table 3 Summary of sample configurations

Sample no.	Matrix material	Discontinuous filler	Infill pattern	Infill percentage (%)	Continuous wire	Nozzle diameter (mm)
1	PLA	None	Unidirectional	100	None	1.0
2	PLA	Copper	Unidirectional	100	None	1.0
3	PLA	None	Unidirectional	100	Copper	1.0
4	PLA	None	Bidirectional	50	Copper	1.0
5	PLA	Copper	Unidirectional	100	Copper	1.0
6	PLA	None	Unidirectional	100	Copper	0.6

required multiple stages of grinding and polishing of the samples. This also allowed for microscopic investigation of the internal structure of the printed samples to understand the wire–polymer configuration and any interaction between the two materials.

The samples went through five stages of grinding and polishing: The samples were first ground with a 60-grit polishing disc using an auto polishing machine (Ultrapol End & Edge Polisher, ULTRA TEC Manufacturing Inc, USA). Thereafter, 180, 280, 600, and 1200/4000 polishing discs were used until a smooth surface was obtained. Figure 3 shows the printed samples after the grinding and polishing process.

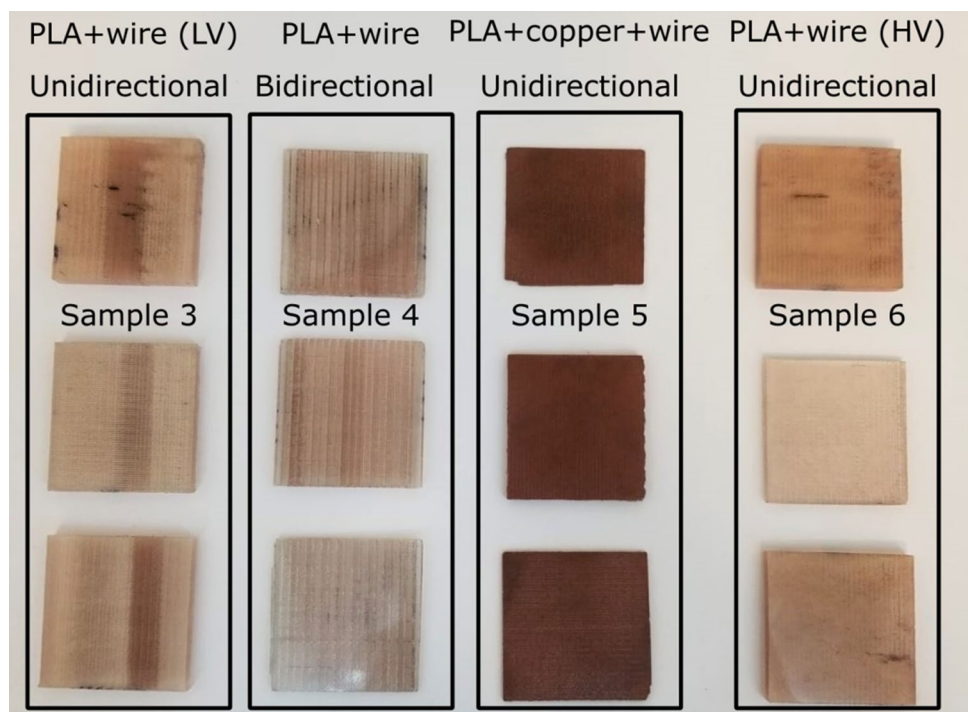
Microscopic imaging was performed using an optical microscope (LEICA MZ10 F, LEICA, Germany). The images were imported into image processing software (ImageJ, National Institutes of Health, Bethesda, Maryland, USA) to quantify the continuous filler content. The images

were firstly thresholded to differentiate the wires from the adjacent polymer. The wire area was measured, and the percentage of the continuous filler was calculated based on the ratio between the wire area and the total area of the sample.

3 Modeling the thermal conductivity of CWPCs

Depending on the filler material, shape, and orientation, an appropriate analytical model can predict the thermal conductivity of polymer composites [18]. One basic model is the rule-of-mixture which describes composite thermal conductivity as a function of only the constituents’ thermal conductivities and volume fractions. Although rule-of-mixture does not account for interfacial resistance between the constituent phases, it can adequately describe CWPC properties, as

Fig. 3. 3D-printed CWPC samples from Table 4 showing wire-reinforced samples with low volume fraction (LV) and high-volume fraction (HV)



shown in the previous study on continuous fiber polymer composites [21].

In CWPCs, the three material phases are the polymer matrix, wires, and air (in the form of voids); these constituents influence the effective thermal conductivity based on their configurations. For the printing configurations used herein, heat transfer through the samples can be described using a network of thermal resistances. These resistances depend on the properties of the different phases and their geometrical configurations with respect to the direction of heat flow.

Conduction heat transfer in solid material is governed by Fourier's Law which for 1D heat flow is

$$Q = kA \frac{\Delta T}{t} \quad (1)$$

where Q is the heat transfer rate, k is thermal conductivity, A is the area normal to heat transfer, and $\Delta T/t$ is the temperature gradient per unit thickness, t .

The 1D thermal resistance of a material is given as

$$R_{thermal} = \frac{\Delta T}{Q} = \frac{t}{kA}. \quad (2)$$

The total thermal resistance of a composite material depends on the configuration of constituent resistances. In the unidirectional samples, when heat flows in the axial direction of the rasters, the thermal circuit is represented as three parallel resistances of polymer, air, and wires, as shown in Fig. 4a. In such configurations, heat tends to flow through the path of least resistance. If heat is conducted perpendicularly through the sample, as shown in Fig. 4b, this results in the resistances being arranged in series and parallel configurations, as in Fig. 4b. The bidirectional samples represent a combination of the previous two configurations, and the corresponding thermal circuit is shown in Fig. 4c.

The equivalent resistance of the configurations shown in Fig. 4 are evaluated by summing these resistances. Because air has a much lower thermal conductivity and volume fraction than the polymer or wire, it can be neglected when it is in parallel with a more conductive material, as in Fig. 4a. As a result, the total resistance of the unidirectional samples when heat is supplied parallel to the wire can be simplified as

$$\frac{1}{R_{parallel}} = \frac{k_{eff}A}{t} = \frac{k_w A_w}{t} + \frac{k_m A_m}{t} \quad (3)$$

where $R_{parallel}$ is the parallel thermal resistance, k_{eff} is the effective thermal conductivity of the composite, A is the nominal cross-sectional, k_w and k_m are the wire and matrix conductivities respectively, A_w and A_m are the wire and matrix cross-sectional areas, respectively, and t is the thickness of the sample.

Equation 3 can be rearranged to obtain the effective thermal conductivity as a function of matrix and wire thermal conductivities and volume fractions, given as

$$k_{eff} = (1 - v_w)k_m + v_w k_w. \text{ Unidirectional model.} \quad (4)$$

where v_w is the volume fraction of wire.

For the bidirectional configuration shown in Fig. 4c, the existence of air with high volume fraction in series with the polymer and wires results in a much higher resistance and minimal heat passes through the perpendicular rasters. As a result, the contribution of the perpendicular rasters can be neglected, and the effective thermal conductivity of the composite can be represented as a function of the wire and polymer volume fraction parallel to the heat flow (v_{wp}), given as

$$k_{eff} = (1 - v_{wp})k_m + v_{wp}k_w \text{ Bidirectional model} \quad (5)$$

To accurately predict the effective thermal conductivity of the CWPC samples, constituent properties should be accurately measured. Elkholy et al. [27] measured the thermal conductivity of PLA and discontinuous copper-filled PLA using the same facility and demonstrated that printing parameters, such as raster width and height can influence thermal conductivity. Thus, the matrix materials used in this study were measured independently to ensure that the printed samples have printing parameters similar to those of the CWPCs. The thermal conductivity of the copper wire was taken as 398 W/mK, according to [28]. The wire and matrix volume fractions were evaluated based on the optical analysis of the filler content.

4 Thermal conductivity measurements

The effective thermal conductivity of the samples was characterized using the apparatus developed in [27], based upon a modified guarded hot plate technique which is an embodiment of ASTM C177 [29]. A schematic of this apparatus is shown in Fig. 5. The apparatus consists of a primary heater block guarded by a secondary heater block and a primary cooling block guarded by a secondary cooler. Thermal power from electrical heaters embedded in the primary heater block was conducted through the sample to the primary cooling block. The secondary blocks were maintained at nearly identical temperatures to the primary blocks to ensure all electrical power to the heaters went through the sample. The steady-state temperature difference across the sample was measured using resistance temperature detectors (RTDs) inserted into each block and the measured thermal resistance of the sample, R_{meas} , can be given by

$$R_{meas} = \frac{(T_{hot} - T_{cold})}{Q} \tag{6}$$

where T_{hot} is the temperature of the primary heater block, T_{cold} is the temperature of the primary cooling block, and Q is the electrical input power to the primary heater block.

The measured thermal resistance consists of the sum of the bulk sample resistance and any thermal contact resistance (R_c) between the sample and the apparatus given by

$$R_{meas} = R_{c,1} + R_{c,2} + R_{sample} = R_c + R_{sample} \tag{7}$$

$$= R_c + \frac{t}{k_{sample}A} \tag{8}$$

From here, the thermal conductivity of the sample can be calculated by rearranging the above as

$$k_{sample} = \frac{t}{A \left[\frac{(T_{hot} - T_{cold})}{Q} - R_c \right]} \tag{9}$$

where t is the thickness of the sample. The contact resistance was quantified by measuring the total thermal resistance for several thicknesses of a given sample and extrapolating the measured resistance to zero thickness.

The primary and secondary (guard) blocks were machined from copper; the primary blocks had a contact area of 40 mm × 40 mm. Cartridge heaters energized by independently controlled DC power supplies (Aim TTI, CPX400D) were used to control the temperature of the primary and secondary heater blocks.

The temperature of all blocks was measured using 1-mm-diameter, 15-mm-long RTDs (Omega, 1PT100KN1510) inserted into holes at the locations shown in Fig. 5; these were calibrated to within 0.01 K of each other.

Temperature measurements were logged using an Agilent 34970A data acquisition system, while the input power to the primary heaters was quantified by measuring the voltage and current using two independent Agilent 34401A digital multimeters. A MATLAB script was customized to record all the measured values and to calculate the time gradient of the measured values. The system was considered at steady state when the time gradient of the temperatures reached 1e–5 K/s.

The input power to the secondary heater was controlled by MATLAB to ensure that the temperature difference between the primary and secondary block did not exceed 0.01 K. This was achieved by varying the power to the secondary heater until its temperature was identical to the primary heater, eliminating the thermal gradient and therefore heat loss from the primary heater.

The sample under test was clamped between the primary and secondary heating and cooling blocks using a clamping

screw, device frame, and load cell (KAF-S, AST, Dresden, Germany), as shown in Fig. 5. Samples were clamped with a pressure of approximately 3 MPa and a few droplets of mineral oil was used to minimize thermal contact resistance and constriction resistance. The entire assembly was encased with silica aerogel insulation which has a thermal conductivity of 0.014 W/mK. Additional details regarding the data acquisition, temperature control, calibration, and uncertainty analysis are provided in [27].

5 Results and discussion

5.1 Microstructure analysis

Figures 6 and 7 show microscopic cross-sectional images of the CWPC (from Table 3) in which the matrix, wires, and air voids can be seen. For Sample 3 (unidirectional using PLA matrix and 1 mm nozzle), the PLA matrix in Fig. 6a appears to achieve better raster adhesion compared with the PLA with copper particles shown in Fig. 6b (Sample 5). Although the two samples were printed with the same printing parameters, bigger air voids and individual rasters can be more clearly seen in the PLA + copper particle matrix. This could be due to a difference in the amount of extruded material because of a slight difference in filament diameters. Another likely reason is due to differences in the rheological properties between the two molten polymer matrices and their interaction with the copper wire during printing.

In the bidirectional sample shown in Fig. 7a, the axial and transverse wires and the air gaps between the axial rasters are visible. Although the rasters have a similar width to those in Fig. 6, the grid-pattern nozzle movement squeezes the previously printed rasters, causing an increase in their thickness and a decrease in their height in this sectional view. The line pattern with the 0.6 mm nozzle shown in Fig. 7b appears to show better adhesion between the rasters with the air voids closer to the wires, compared with the 1 mm nozzle.

Based on the area ratio, the continuous filler content was obtained. Table 4 summarizes the filler content for the different samples. The wire volume fraction of the bidirectional sample was calculated based on the area of the wires

Table 4 Wire volume fraction based on the image processing

Sample no	Wire volume fraction (v_{wp}) %
3	1.07
4	0.538
5	1.07
6	2.7

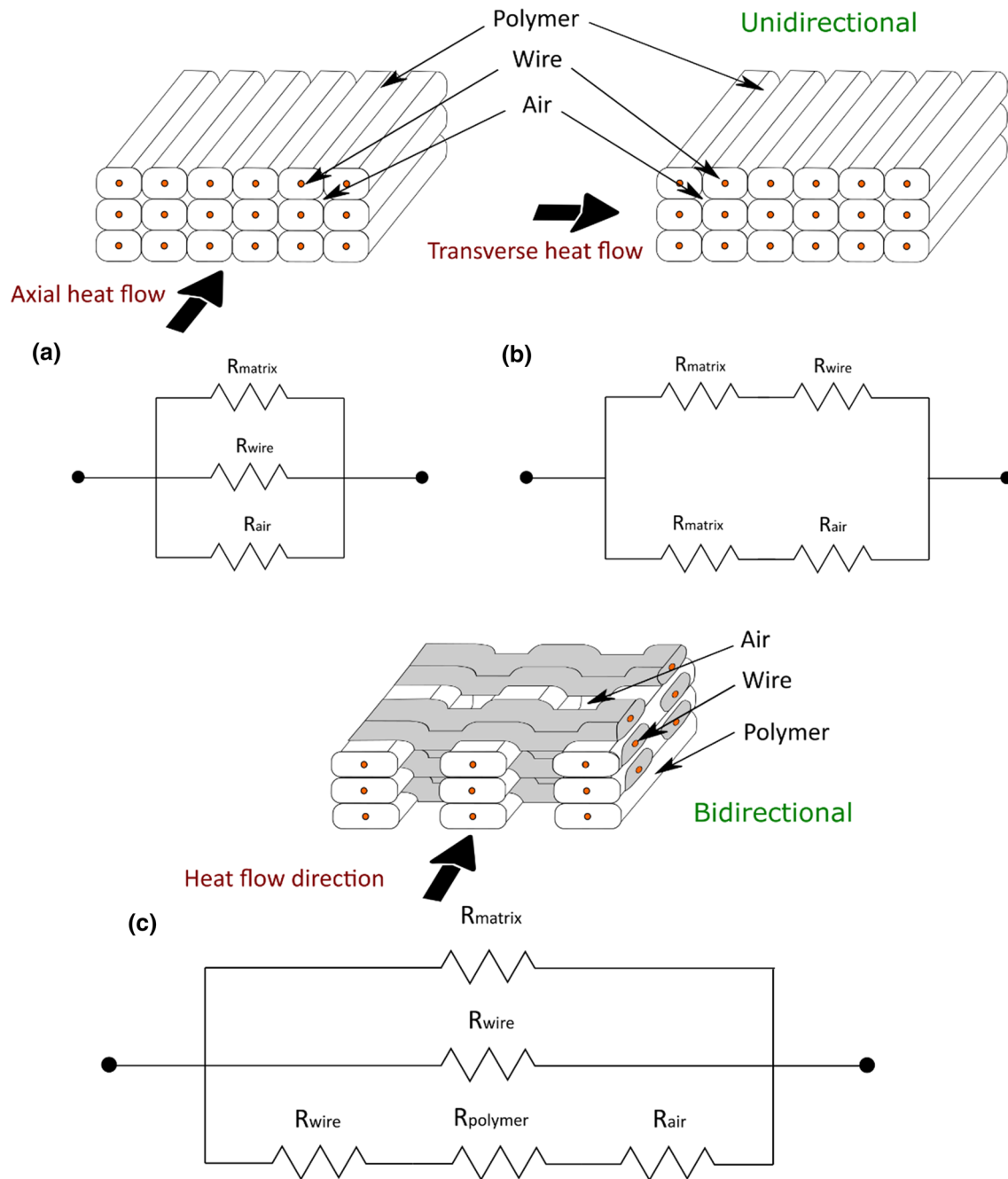


Fig. 4 Schematic diagram for thermal circuit of unidirectional samples: (a) axial heat flow, (b) transverse heat flow, and (c) bidirectional samples

perpendicular to the cross-section, which represents the wires parallel to the heat transfer direction.

5.2 Effective thermal conductivity

Thermal conductivity measurements were performed using the setup described in Sect. 4. After polishing, each sample was tested before going through another set of grinding and

polishing stages to reduce thickness. Thermal resistance of three or four thicknesses was measured for each sample.

The PLA and copper-filled PLA samples were tested first to evaluate their thermal conductivities and to use these values as inputs in the analytical models in order to predict the effective thermal conductivity of the CWPC samples. For example, the input power to the heaters for the PLA sample was 0.5 W which resulted in temperature differences across the sample of 6.2 K, 4.7 K, and 3.03 K

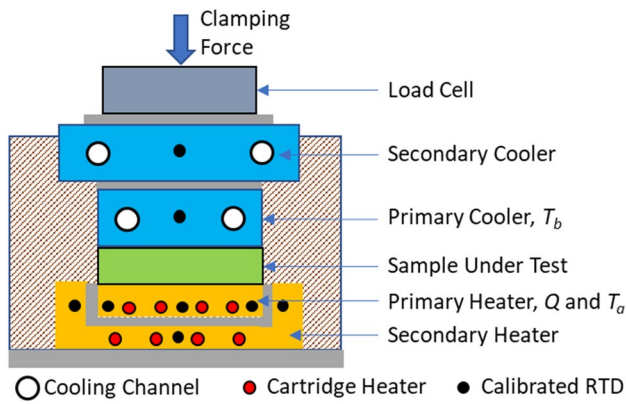


Fig. 5 Schematic of thermal conductivity apparatus

at 4.09 mm, 3.07 mm, and 2.02 mm thicknesses, respectively. The measured thermal resistance of each thickness was evaluated using Eq. 2 and plotted against the sample thickness, as shown in Fig. 8. Thereafter, the trend line for the measured points was obtained using a linear regression fit. The discontinuous copper-filled PLA sample was processed similarly, and its R_{meas} vs thickness is also plotted in Fig. 8.

The linear best fit lines in Fig. 8 correspond to Eq. 8, and their intersections with the y-axis represent the contact resistance between the samples and the apparatus. The slope of the curve is the inverse of the sample thermal conductivity and area ($1/kA$). For PLA and copper-filled PLA, the contact resistance was less than 3% of the total measured resistance at the smallest thickness. This is consistent

with observations by Elkholy et al. in [27] for materials with low thermal conductivity.

The copper-filled PLA of Sample 2 yielded a thermal conductivity of 0.5 W/mK compared with 0.22 W/mK for the pure PLA Sample 1. Although the composite matrix was 80% filled with copper particles, the effective thermal conductivity appears to be dominated by the polymer conductivity. This improvement in conductivity comes at the expense of weight: the copper-filled PLA had a relatively high density ($\approx 3.5 \text{ g/cm}^3$) which is greater than some conductive metals, such as aluminum ($\approx 2.7 \text{ g/cm}^3$), and thus it is questionable how useful it is for lightweight thermal applications.

The same testing procedure was followed to evaluate the thermal conductivity of the CWPC samples (Samples 3–6). Figure 9 shows the relationship between measured thermal resistance and the specimen thickness for three replicates of the CWPC samples.

Generally, the CWPCs exhibited higher contact resistance than Sample 1 or 2, resulting in a larger temperature drop across the samples. Uncertainty in contact resistance can greatly affect the thermal conductivity calculated from Eq. 8. For this reason, three or four thicknesses of each replicate were tested to evaluate repeatability. The thermal conductivity of each sample was evaluated separately using Eq. 9, and the average value for the three replicates was calculated. Generally, the results showed good linearity with an R^2 greater than 0.98 for all samples.

Figure 9a shows the relation between the total resistance and the specimen thickness for the unidirectional PLA + wire sample (Sample 3). Here, the contact resistance represented

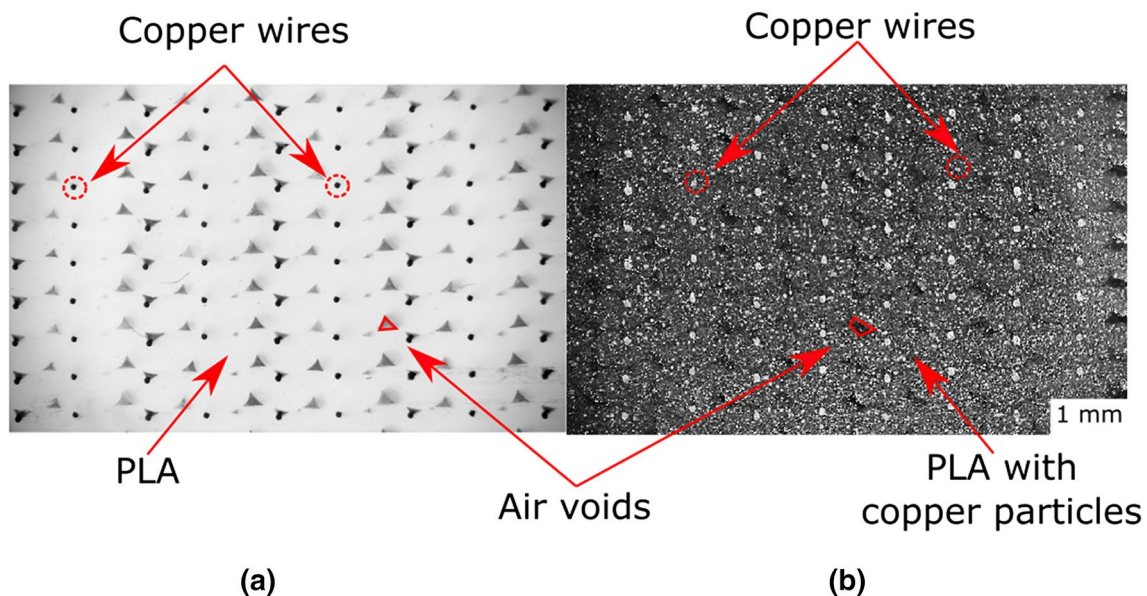


Fig. 6 Cross-sectional view of (a) Sample 3 (unidirectional CWPC using 1 mm nozzle) and (b) Sample 5 (unidirectional PLA + copper particle CWPC using 1 mm nozzle)

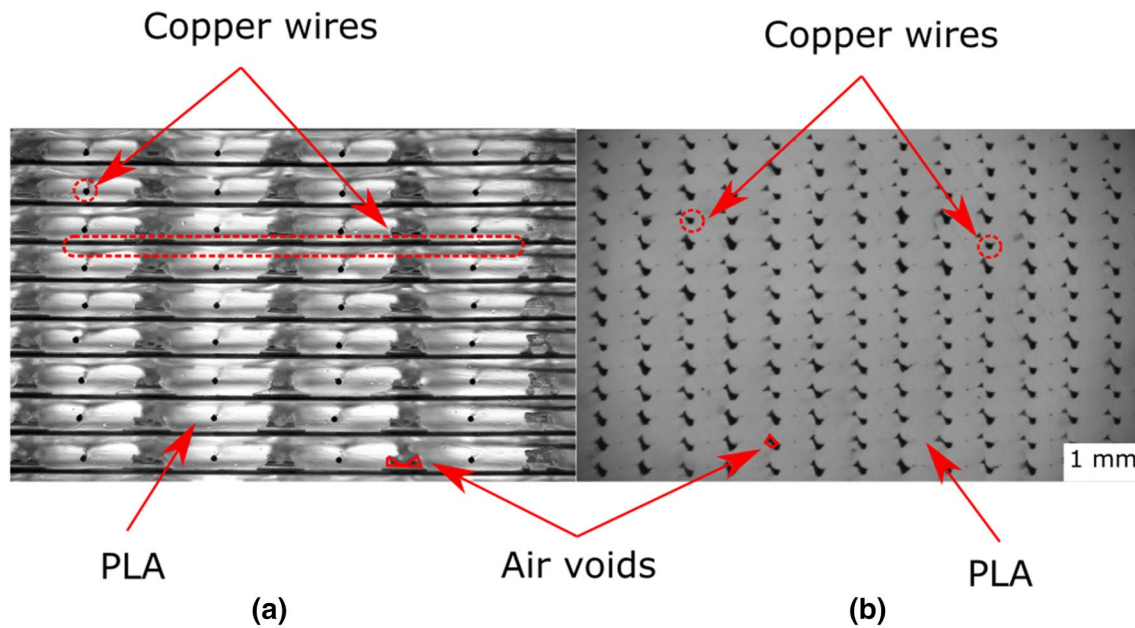


Fig. 7 Cross-sectional view of (a) Sample 4 (bidirectional PLA CWPC using 1 mm nozzle) and (b) Sample 6 (unidirectional PLA CWPC using 0.6 mm nozzle)

approximately 40% of the total resistance of the thinnest sample.

For the bidirectional samples (Sample 4), higher contact resistance was measured, with the contact resistance contributing 68% of the total measured resistance for the thinnest sample, as shown in Fig. 9b. The increased contact resistance for this sample is due to the grid printing pattern, which results in more air voids within the sample, as seen in Fig. 7. Increased air voids in contact with the heating and cooling

blocks of the apparatus serve to increase contact resistance for these samples.

The unidirectional PLA + copper + wire samples (Sample 5) had a similar configuration to the PLA + wire (Sample 3) and the same wire volume fraction. Although the values of the contact resistance for copper-filled matrix with wires were lower compared with the PLA + wire, the bulk resistance values were also lower, causing a more pronounced effect of contact resistance on the total measured resistance, as shown in Fig. 9c. The variation in the contact resistance between the replicates is thought to be caused by irregularities in the grinding and polishing processes. However, the linearity of the trend lines shows that these irregularities are consistent for the same replicate.

The measured resistance of the PLA + wire samples with the highest wire volume content (Sample 6) is plotted against its thickness in Fig. 9d. These replicates had the highest thermal conductivities (and therefore lowest bulk resistances); therefore, contact resistance was found to have the most significant effect on total measured resistance, accounting for 85% of the lowest measured resistance. Despite this, the thermal conductivity, which is derived from the slopes of these curves, was relatively consistent.

Figure 10 summarizes the total specific contact resistance (RA) values for the matrix and the wire-reinforced samples. It is important to note that these values represent the sum of the two contact resistances from both sides of the sample (i.e., $R_{c,1} + R_{c,2}$ in Eq. 7). The uncertainty of the contact resistance in the CWPC samples was calculated as twice the standard deviation of the values from the three replicates.

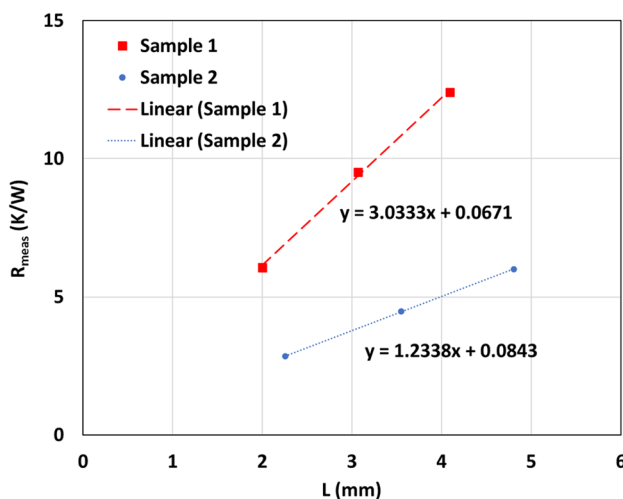


Fig. 8 Measured resistance against sample thickness for PLA sample (Sample 1) and PLA + Copper (Sample 2)

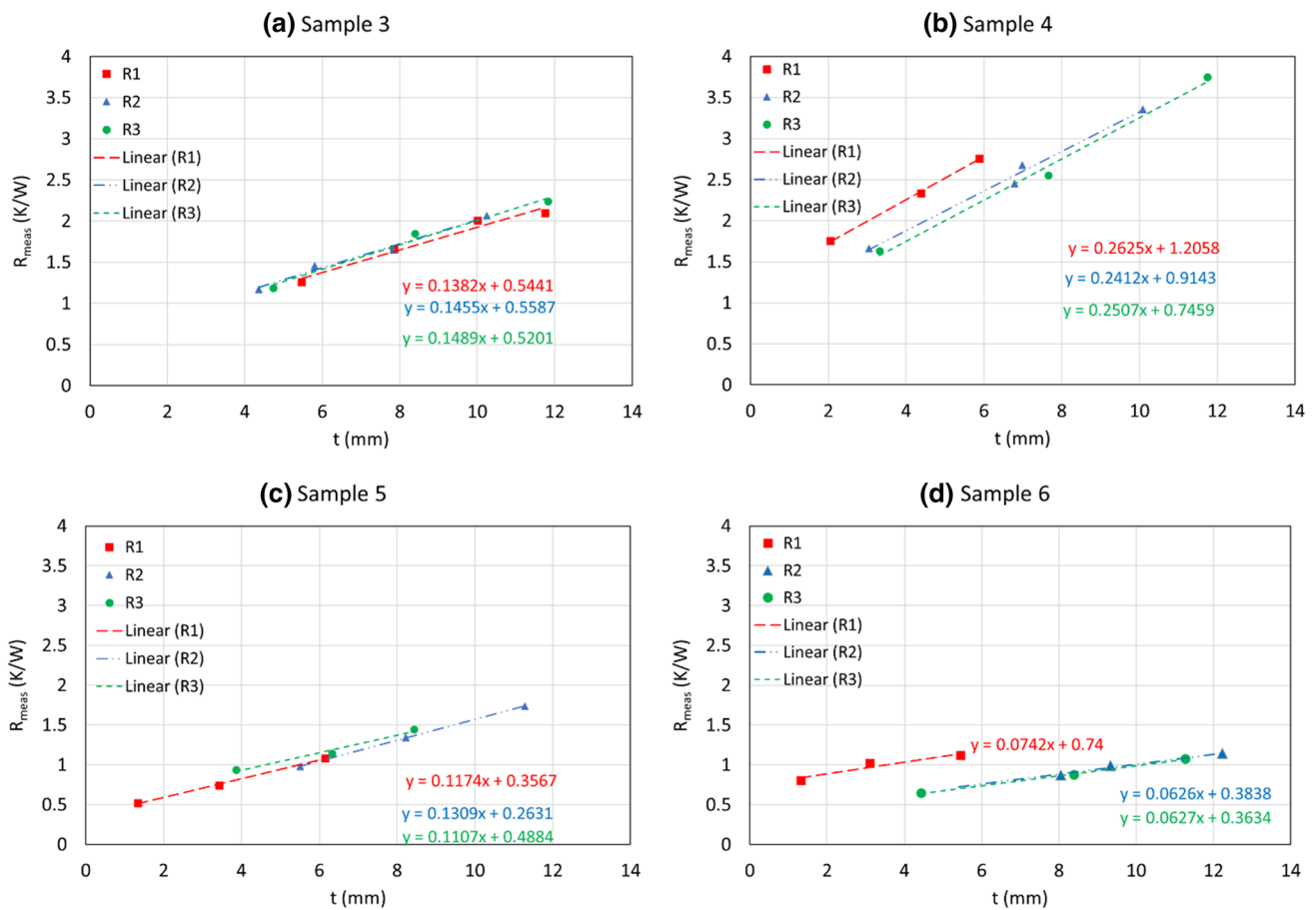


Fig. 9 Measured thermal resistance as a function of thickness for three replicates (R1–3) of (a) Sample 3 (Unidirectional PLA + wire), (b) Sample 4 (Bidirectional PLA + wire), (c) Sample 5 (Unidirectional PLA + copper + wire), (d) Sample 6 (Unidirectional PLA + wire)

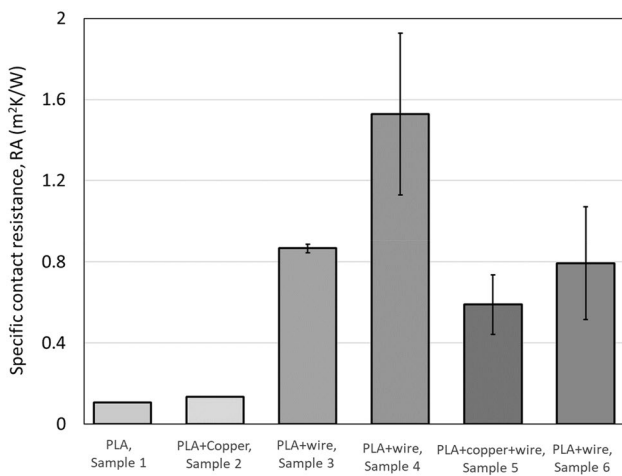


Fig. 10 Summary of total specific contact resistance (both sides) of all samples

Here, Samples 1 and 2 (PLA and PLA + copper), which do not contain copper wires, exhibit the lowest contact resistance. The CWPC samples (Samples 3–6) exhibit significantly more resistance; it is suggested that this increase is due to the relatively harder copper wires contacting the interface. It can be deduced from Fig. 12 that the contact area of the solid phase greatly affects the contact resistance. This can be seen in the bidirectional sample (Sample 4) which had the lowest solid contact with the measurement test rig and the highest contact resistance. This sample also exhibited high uncertainty because the ratio of copper wires to polymer at the cross-sections was variable because of the bidirectional wires. The unidirectional CWPC samples (Samples 3, 5, and 6) have more consistent cross-sections and therefore similar contact resistance values.

Figure 11 shows a summary of thermal conductivity for all samples. Sample 3, which had a unidirectional configuration and only 1.07% of continuous wire, had a thermal conductivity of 4.47 W/mK which represents a factor of 21 increase in thermal conductivity when compared with pure PLA (Sample 1). The parallel resistance model prediction

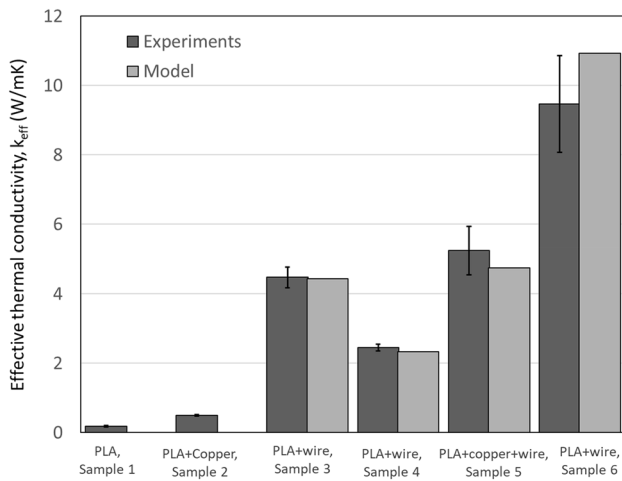


Fig. 11 Summary of thermal conductivities of matrix materials and CWPC samples

plotted in Fig. 11 predicts a thermal conductivity of 4.44 W/mK, which is consistent with the experimental results. Sample 4 (bidirectional configuration) showed an effective thermal conductivity of almost half of unidirectional Sample 3, as predicted by the model. The samples printed with the PLA matrix had a similar density to the pure PLA because the wire content was very small (1.07%). This means that, compared with the copper-filled PLA, CWPC significantly improves thermal conductivity without losing lightweight advantage, albeit only in the direction of the wires.

The copper-particle matrix with wires (Sample 5) exhibited a slightly higher effective thermal conductivity (5.2 W/mK) than Sample 3 and was also slightly higher than the model prediction. It is not clear that there was any thermal communication between the discontinuous copper particles and the copper wires, and the slightly improved thermal

conductivity (compared with Sample 3) is primarily attributed to the more conductive matrix.

By increasing the wire volume content to 2.7% (Sample 6), the thermal conductivity of the unidirectional CWPC increased to 9.4 W/mK, which represents a pure polymer conductivity increase of almost 50 fold. The high uncertainty associated with Sample 6 is caused by a difference in contact resistance across the replicates, which may have occurred due to inconsistent contact surfaces during the grinding and polishing stages (Fig. 9d). Testing additional replicates and ensuring similar surface finishing may help reduce this uncertainty.

These results address primarily the in-plane thermal conductivity where heat transfer is in the direction of the wires. Based on the consistent thermal network model predictions for unidirectional and bidirectional samples, we do not expect the through-plane conductivity of these samples much higher than that of the base polymer matrix because the copper wires are entirely in series with the heat flow. That said, 3D-printing could allow for more complex and application-tailored heat flow paths within each layer.

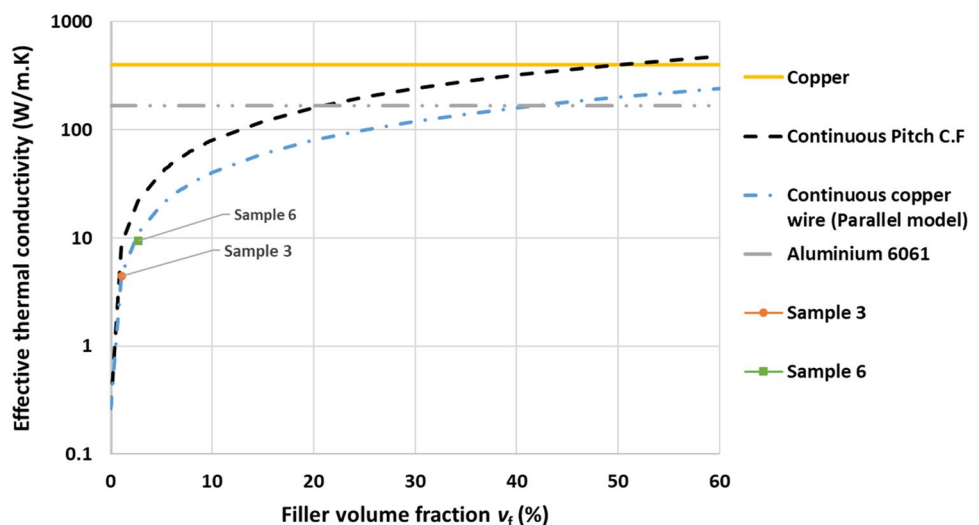
6 Summary and outlook

3D-printed CWPCs were manufactured and characterized experimentally to investigate the effect of wire content, orientation, and matrix material on thermal conductivity and contact resistance.

The effective thermal conductivity of the printed composites was measured experimentally and predicted analytically using a simple thermal resistance network model.

Multiple thicknesses for each sample were tested to characterize the effect of contact resistance on the measured

Fig. 12 Predicted effective thermal conductivities as a function of volume fraction using continuous conductive wires or pitch carbon fibers



thermal resistance. Generally, contact resistance increased with wire area fraction at the contacting surfaces.

The thermal conductivity of a copper-filled discontinuous PLA matrix (80% copper particles) had a thermal conductivity almost 2.5 times that of pure PLA. By introducing continuous copper wire into the composite (1.07% volume content of copper wire), the thermal conductivity increased to 23 times the thermal conductivity of the base polymer. When copper-filled PLA was used, the thermal conductivity of the composite increased to 27 times that of pure PLA.

The orientation of the conductive wires had a significant effect on the thermal conductivity and the highest thermal conductivity was obtained when the wires were aligned in the heat transfer direction. Printing with a bidirectional pattern reduced the thermal conductivity to almost half of the unidirectional sample, which is consistent with the predictions of the network resistance model. The model predictions further suggest that through-plane conductivity of these CPWCs would be on a similar order as the base polymer matrix.

These results demonstrate the potential of 3D-printed CWPCs as components in polymer-based heat exchanger applications where historically the thermal conductivity of the solid phase can be a limiting performance factor. Further improvement to printing processes can be incorporated to allow for higher volume fraction of wires. This could include a wire-feeding mechanism to overcome the need for large quantities of polymer to pull wires out of the nozzle.

Another option would be to employ high-conductivity continuous fibers, such as pitch-based carbon fibers ($k = 800 \text{ W/mK}$ [21]) and carbon nanotubes, to further increase effective thermal conductivity. The foregoing results validate the simple parallel thermal resistance network model to predict effective thermal conductivity of the CWPCs in the direction of the fibers. This model can be extended to predict effective thermal conductivity for other fibers and fill ratios. Figure 12 shows anticipated thermal conductivity with respect to filler volume fraction using the parallel model. Here, a thermal conductivity of 167 W/mK (similar to aluminum alloy 6061 which is commonly used for heat sink applications) could be achieved with continuous fiber polymer composite with only 20% pitch-based carbon fibers.

These conductivity improvements comprise an important step toward realizing the full potential of 3D printing in the fabrication of complex-shaped, high-performance 3D-printed composite heat exchange technologies.

Acknowledgements The authors acknowledge the support of the Natural Sciences and Engineering Research Council of Canada (NSERC).

Funding Natural Sciences and Engineering Research Council of Canada, grant no. RGPIN-2018-05879.

Declarations

Conflict of interest On behalf of all authors, the corresponding author states that there is no conflict of interest.

References

- Jafari D, Wits WW (2018) The utilization of selective laser melting technology on heat transfer devices for thermal energy conversion applications: a review. *Renew Sustain Energy Rev* 91(June):420–442. <https://doi.org/10.1016/j.rser.2018.03.109>
- Deisenroth DC, Moradi R, Shoostari AH, Singer F, Bar-Cohen A, Ohadi M (2018) Review of heat exchangers enabled by polymer and polymer composite additive manufacturing. *Heat Transfer Eng* 39(19):1648–1664. <https://doi.org/10.1080/01457632.2017.1384280>
- Wang X, Jiang M, Zhou Z, Gou J, Hui D (2017) 3D printing of polymer matrix composites: a review and prospective. *Compos Part B Eng* 110:442–458
- Kalsoom U, Nesterenko PN, Paull B (2016) Recent developments in 3D printable composite materials. *RSC Adv* 2016(6):60355–60371. <https://doi.org/10.1039/C6RA11334F>
- Sa'ude N, Masood SH, Nikzad M, Ibrahim M, Ibrahim MHI (2013) Dynamic mechanical properties of Copper–ABS composites for FDM feedstock. *Int J Eng Res Appl* 3:1257–1263
- Nikzad M, Masood SH, Sbarski I (2011) Thermo-mechanical properties of a highly filled polymeric composites for Fused Deposition Modeling. *Mater Des* 32(6):3448–3456
- Masood SH, Song WQ (2004) Development of new metal/polymer materials for rapid tooling using Fused deposition modelling. *Mater Des*. <https://doi.org/10.1016/j.matdes.2004.02.009>
- Masood SH, Song WQ (2005) Thermal characteristics of a new metal/polymer material for FDM rapid prototyping process. *Assem Autom* 25(4):309–315. <https://doi.org/10.1108/01445150510626451>
- Hwang S, Reyes EI, Moon Ks et al (2015) Thermo-mechanical characterization of metal/polymer composite filaments and printing parameter study for fused deposition modeling in the 3D printing process. *J Elec Mater* 44:771–777. <https://doi.org/10.1007/s11664-014-3425-6>
- Brenken B, Barocio E, Favaloro A, Kunc V, Pipes RB (2018) Fused filament fabrication of fiber-reinforced polymers: a review. *Addit Manuf* 21(January):1–16
- Zhong W, Li F, Zhang Z, Song L, Li Z (2001) Short fiber reinforced composites for fused deposition modeling. *Mater Sci Eng A* 301(2):125–130. [https://doi.org/10.1016/S0921-5093\(00\)01810-4](https://doi.org/10.1016/S0921-5093(00)01810-4)
- Ning F, Cong W, Hu Y, Wang H (2017) Additive manufacturing of carbon fiber-reinforced plastic composites using fused deposition modeling: effects of process parameters on tensile properties. *J Compos Mater* 51(4):451–462
- Ivey M, Melenka GW, Carey JP, Ayranci C (2017) Characterizing short-fiber-reinforced composites produced using additive manufacturing. *Adv Manuf Polym Compos Sci* 3(3):81–91
- Bagchi A, Nomura S (2006) On the effective thermal conductivity of carbon nanotube reinforced polymer composites. *Compos Sci Technol*. <https://doi.org/10.1016/j.compscitech.2005.11.003>
- Lee GW, Lee JI, Lee SS et al (2005) Comparisons of thermal properties between inorganic filler and acid-treated multiwall nanotube/polymer composites. *J Mater Sci* 40:1259–1263. <https://doi.org/10.1007/s10853-005-6947-8>
- Lee GW, Park M, Kim J, Lee JI, Yoon HG (2006) Enhanced thermal conductivity of polymer composites filled with hybrid filler.

- Compos Part A Appl Sci Manuf. <https://doi.org/10.1016/j.compositesa.2005.07.006>
17. Berman R (1976) Thermal conduction in solids. Clarendon press, Oxford
 18. Chen H, Ginzburg VV, Yang J, Yang Y, Liu W, Huang Y, Du L, Chen B (2015) Thermal conductivity of polymer-based composites: fundamentals and applications. *Prog Polym Sci* 59:41–85
 19. Prasher R (2009) Acoustic mismatch model for thermal contact resistance of van der Waals contacts. *Appl Phys Lett* 94(4):1–4
 20. Pietrak K, Wiśniewski TS (2014) Methods for experimental determination of solid-solid interfacial thermal resistance with application to composite materials. *J Power Technol* 94(4):270–285
 21. Ibrahim Y, Elkholy A, Schofield J, Melenka GW, Kempers R (2020) Effective thermal conductivity of 3D-printed continuous fiber polymer composites. *Adv Manuf Polym Compos Sci* 6:17–28
 22. Ghosh B, Yousef W, Al Jaber M, Al Hajeri N, Al Braiki A, Evely V, Rodgers P (2016) Design and investigation into the thermal and mechanical performance of a polymer composite prototype gas–liquid heat exchanger. *Int J Thermal Environ Eng* 11:51–59
 23. Ibrahim Y, Melenka GW, Kempers R (2018) Additive manufacturing of continuous wire polymer composites. *Manuf Lett* 16(April):49–51
 24. Ibrahim Y, Melenka GW, Kempers R (2018) Fabrication and tensile testing of 3D printed continuous wire polymer composites. *RPJ* 24:1131–1141. <https://doi.org/10.1108/RPJ-11-2017-0222>
 25. Saleh M, Kempers R, Melenka GW (2019) 3D printed continuous wire polymer composites strain sensors for structural health monitoring. *Smart Mater Struct* 28:10541
 26. Ibrahim Y, Kempers R, Amirfazli A (2019) “3D printed electro-thermal anti- or de-icing system for composite panels. *Cold Reg Sci Technol* 166:102844. <https://doi.org/10.1016/j.coldregions.2019.102844>
 27. Elkholy A, Rouby M, Kempers R (2019) Characterization of the anisotropic thermal conductivity of additively manufactured components by fused filament fabrication. *Prog Addit Manuf* 4:497–515
 28. MATWEB (2017) Material properties by MATWEB. Available: <http://www.matweb.com>. Accessed 11 Aug 2021
 29. ASTM C1777 (2013) Standard test method for steady-state heat flux measurements and thermal transmission properties by means of the guarded-hot-plate. *ASTM Int* 2013:1–23. <https://doi.org/10.1520/C0177-13.2>”

Publisher's Note Springer Nature remains neutral with regard to jurisdictional claims in published maps and institutional affiliations.